NANO LETTERS

pubs.acs.org/NanoLett

Letter

Robust Room-Temperature Ferroelectricity in β-Bi_2SeO_5 Thin Films

Wei Li, Lingyuan Kong, Kai Hu, Long Chen, Tianci Hu, Zeguo Lin, Yi Jiang, Fang Yang, Jiandong Guo, Yang Guo, Wei Zhang, Runzhang Xu,* Pan Chen,* Yan Liang,* and Jiandi Zhang*

Cite This: https://doi.org/10.1021/acs.nanolett.6c03261

Read Online

ACCESS | Metrics & More | Article Recommendations | Supporting Information

ABSTRACT: Atomic-scale two-dimensional (2D) ferroelectrics are garnering immense research interest for powering next-generation high-performance nanoelectronics. Herein, we report the discovery of robust room-temperature out-of-plane ferroelectricity in thin 2D β-Bi_2SeO_5 films, with the ferroelectric response persisting even down to the monolayer limit. The ferroelectricity of a 10 nm thick β-Bi_2SeO_5 thin film was also unambiguously revealed by ferroelectric analysis using a ferroelectric analyzer, achieving an out-of-plane polarization of 10 $\mu C/cm^2$. Furthermore, a pronounced in-plane ferroelectricity and photoelectric effect were also observed, along with a strong coupling between them. First-principles density functional theory calculations identify the displacement and distortion of [SeO_3] tetrahedra under external electric fields as the primary origin of the observed out-of-plane and in-plane ferroelectric polarization in β-Bi_2SeO_5 films. These findings open up new possibilities for using β-Bi_2SeO_5 thin films in future nanoscale electronic and quantum devices.

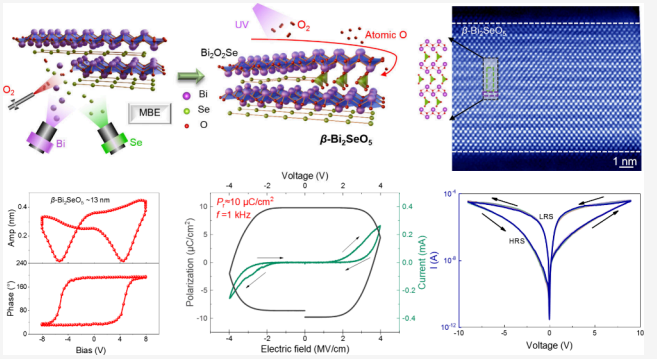

KEYWORDS: *Two-dimensional ferroelectric, β-Bi_2SeO_5, Molecular beam epitaxy, Oxidation reaction, Thin film, Oxides*

Ferroelectric (FE) materials, which exhibit switchable electrical polarizations under external electric fields[1−3] have demonstrated significant potential in a variety of applications, including non-volatile memories[4−6] FE field-effect transistors[7−10] transducers[11,12] actuators[13,14] and so on. Ferroelectricity is conventionally observed in noncentrosymmetric materials[1,15,16] such as three-dimensional (3D) perovskite oxides including $BaTiO_3$,[17] $PbTiO_3$,[18] $BiFeO_3$,[19] and $LiNbO_3$.[20] Given the ongoing trend towards miniaturization in microelectronic devices, the impact of thickness on FE thin films has emerged as a critical scientific issue.[21] In 3D perovskite oxides, the depolarization field generated by surface-bound charges can substantially diminish or even completely suppress ferroelectricity when the film thickness decreases to a critical nanoscale dimension.[22] For instance, when the thickness of $PbTiO_3$ thin films is reduced to 3 unit cells, ferroelectricity is markedly suppressed and the Curie temperature decreases significantly.[23] In contrast to traditional 3D FE materials, two-dimensional (2D) materials exhibit a layered structural characteristic: the intralayer is composed of strong covalent bonds forming a rigid lattice, while interlayers are bound only through weak van der Waals forces or electrostatic interactions[3,24] This unique structural characteristic ensures the preservation of lattice integrity even at remarkably thin dimensions, providing a foundational basis for sustained stable ferroelectricity.

2D FE materials present several advantages: their lack of dangling bonds grants them superior mechanical flexibility, facilitating integration with other 2D materials to produce atomically flat interfaces ideal for multifunctional devices;[25−27] moreover, their thickness, typically under 3 nm, makes them perfect candidates for future high-integration, energy-efficient information processing and storage systems.[6,28−30] To date, a variety of 2D FE materials have been identified, such as $CuInP_2S_6$,[31] $CuCrP_2S_6$,[32] α-In_2Se_3,[33] NiI_2,[34] group IV chalcogenides (e.g., SnTe,[35] GeTe[36]), transition metal chalcogenides (e.g., WSe_2,[37] 1T-$MoTe_2$[38]), and bismuth-based oxychalcogenides (e.g., Bi_2O_2Se,[39−41] α-Bi_2SeO_5[7]). Among these, bismuth-based oxychalcogenides are particularly promising owing to their superior properties. For instance, analogous to Si/SiO_2 system, FE high-k native dielectric, α-Bi_2SeO_5, can be accurately synthesized on top of high-mobility Bi_2O_2Se semiconductor, resulting in atomic interfaces.[7,42,43] Field-effect transistors fabricated directly with α-Bi_2SeO_5 as the gate dielectric demonstrate mobility exceeding 300 $cm^2/V{\cdot}s$ and on/off current ratios approaching 10^6.[44]

In addition to α-Bi_2SeO_5, single-crystal β-Bi_2SeO_5 is another well-known high-k dielectric among bismuth-based oxy-

Received: July 2, 2026
Revised: August 26, 2026
Accepted: August 28, 2026

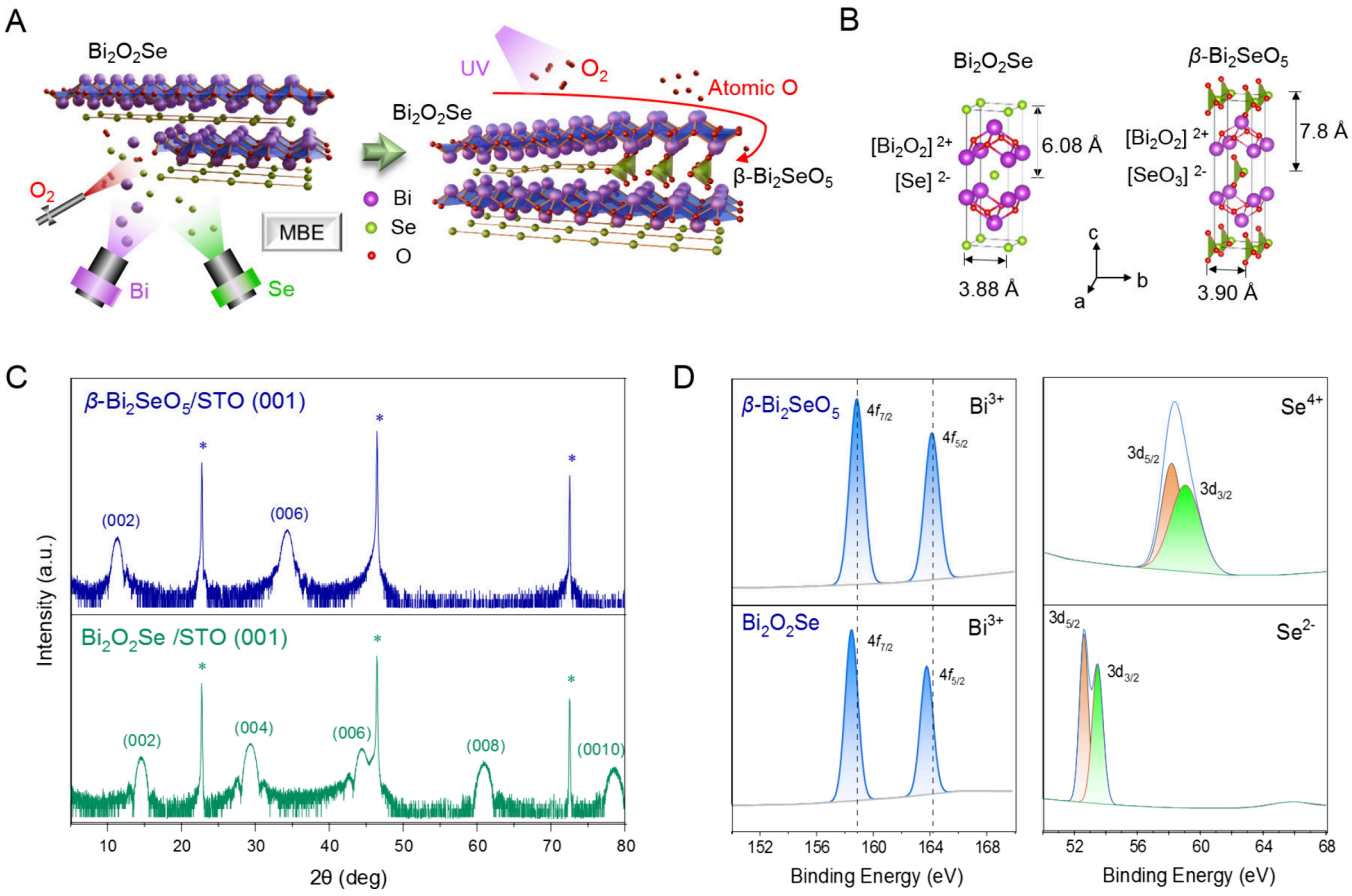

Figure 1. Crystal structure and physical characterization of β-Bi_2SeO_5 and Bi_2O_2Se films. A) The schematic diagram of the growth of a Bi_2O_2Se film using MBE, followed by the process of intercalating atomic oxygen into Bi_2O_2Se to form β-Bi_2SeO_5 through ultraviolet exposure. B) The crystal structures of Bi_2O_2Se and β-Bi_2SeO_5. C) XRD pattern of Bi_2O_2Se (bottom) and β-Bi_2SeO_5 (top). The asterisks indicate the peaks of $SrTiO_3$ substrates. D) XPS spectra of Bi and Se elements in Bi_2O_2Se (bottom) and β-Bi_2SeO_5 (top).

chalcogenides that can also form an atomically sharp interface with a Bi_2O_2Se film.[45] β-Bi_2SeO_5 is characterized by a wide bandgap of ~3.25 eV and a high dielectric constant of approximately 22, indicating its potential for application as the dielectric layer in nanodevices.[46] Field-effect transistors constructed using β-Bi_2SeO_5 in a 2D gate-all-around configuration have demonstrated performance surpassing the physical limitations of existing commercial silicon-based transistors in terms of both speed and energy efficiency.[47] As β-Bi_2SeO_5 is a low-temperature phase that can only be synthesized at temperatures up to approximately 340 °C, it is difficult to grow uniform 2D films via conventional growth methods; instead, it must be transformed from a 2D Bi_2O_2Se precursor via an ultraviolet-assisted intercalative oxidation method[45,46,48] Therefore, the quality of the resulting β-Bi_2SeO_5 is entirely dependent on the quality of the parent Bi_2O_2Se film. At present, 2D Bi_2O_2Se can be synthesized using various methods such as chemical vapor deposition,[44] molecular beam epitaxy (MBE)[41,49] pulsed laser deposition,[50] and metal-organic vapor phase epitaxy.[51] Among these techniques, the MBE method for fabricating Bi_2O_2Se thin films offers notable advantages: it allows for precise control of film thickness ranging from monolayer to multilayer scales, ensures low defect density, and exhibits excellent scalability. The MBE-grown Bi_2O_2Se films will enable more precise control over the β-Bi_2SeO_5 film formation. Furthermore, the lack of study on the FE and photoelectric properties of 2D β-Bi_2SeO_5 currently impedes its potential application in future electronic devices.

In this study, we precisely grew scalable, thickness-controlled ultrathin Bi_2O_2Se films on $SrTiO_3$ substrates using the MBE method, which were subsequently converted to β-Bi_2SeO_5 thin films via ultraviolet-assisted intercalative oxidation. We report for the first time the out-of-plane ferroelectricity in β-Bi_2SeO_5 films with thicknesses as low as 1 unit cell (1-UC). The ferroelectricity of a 10 nm thick β-Bi_2SeO_5 film was also unambiguously revealed by FE analysis using a FE analyzer, achieving an out-of-plane polarization of 10 $\mu C/cm^2$. Furthermore, a detailed analysis of the in-plane electronic properties under visible light and laser illumination reveals a pronounced in-plane FE and photoelectric effect and a strong coupling between them. First-principles density functional theory (DFT) calculations suggest that the displacement and distortion of $[SeO_3]$ tetrahedra under electric field are primarily responsible for the observed out-of-plane and in-plane FE polarization of the β-Bi_2SeO_5 films. Our results give rise to new possibilities for using β-Bi_2SeO_5 thin films in nanoscale electronic and quantum devices.

We employed an ultra-high vacuum MBE system to grow high-quality Bi_2O_2Se thin films, followed by post-treatment using ultraviolet ozone intercalation oxidation for the fabrication of β-Bi_2SeO_5 thin films (Figure 1A). Bi_2O_2Se is composed of strongly covalently bonded $[Bi_2O_2]$ layers and planar $[Se]$ layers, exhibiting relatively weak electrostatic

https://doi.org/10.1021/acs.nanolett.6c03261
Nano Lett. XXXX, XXX, XXX−XXX

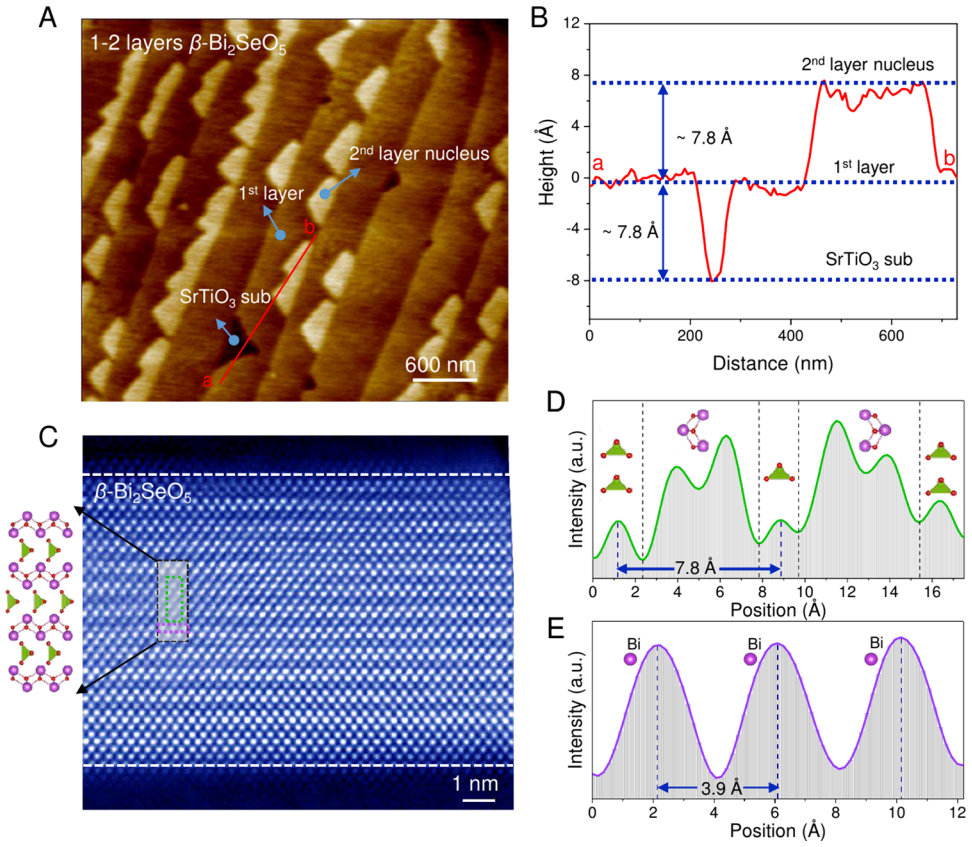

Figure 2. Fine structure characterization of β-Bi_2SeO_5 films. A) AFM surface morphology of the β-Bi_2SeO_5 film with 1-2 layers. B) Height profiles along the red line in panel A. The labels on the curve indicate the $SrTiO_3$ substrate, 1st layer and 2nd layer nucleus of β-Bi_2SeO_5. C) Cross-sectional HAADF-STEM image of the β-Bi_2SeO_5 film, together with its atomic structure model. D, E) Intensity distribution maps obtained along the green and purple rectangular regions in panel C. The results show that the layer thickness of β-Bi_2SeO_5 is 7.8 Å and the in-plane lattice constant is 3.9 Å.

interaction (space group *I*4/*mmm*). The in-plane lattice constant is 3.88 Å, while the out-of-plane interlayer spacing is 6.08 Å (Figure 1B). The primary reaction mechanism during oxidation involves the generation of atomic oxygen from atmospheric oxygen under ultraviolet irradiation. This atomic oxygen then serves as the direct oxidizing agent for intercalation oxidation. During this process, the $[Bi_2O_2]$ framework of the precursor Bi_2O_2Se remains unchanged and O atoms bond with Se^{2-} ions to form $[SeO_3]$ tetrahedra. Accordingly, the interlayer space expands to 7.8 Å (Figure 1B).

For the MBE growth of Bi_2O_2Se films, $SrTiO_3$, which features a cubic structure (a = 3.90 Å) and high thermal stability, was selected as the epitaxial substrate. $SrTiO_3$ exhibits excellent lattice matching with Bi_2O_2Se, exhibiting a lattice mismatch rate of approximately 0.6%. By optimizing growth conditions, Bi_2O_2Se films with atomically flat surfaces and controllable thickness can be obtained. The bottom panel of Figure 1C presents the X-ray diffraction (XRD) results of a representative Bi_2O_2Se thin film with a thickness of approximately 7 nm. Following ultraviolet oxidation treatment at 120°C for 30 min, layered *c*-axis orientated β-Bi_2SeO_5 films were obtained (the top panel of Figure 1C). Sharp diffraction peaks and distinct Laue oscillations observed in the XRD patterns confirm the high crystalline quality and layer-by-layer structure of the β-Bi_2SeO_5 films. X-ray photoelectron spectroscopy (XPS) technique was employed to determine the elemental composition and chemical bonding states of Bi and Se, both pre and post oxidation. In the Bi_2O_2Se film (bottom panel of Figure 1D), peaks at 158.46 eV and 163.75 eV were observed for Bi $4f_{7/2}$ and $4f_{5/2}$, respectively, indicating a valence state of Bi^{3+}. The fitted signals of Se $3d_{5/2}$ and $3d_{3/2}$ located at 52.60 eV and 53.45 eV, respectively, indicated a valence state of Se^{2-}. Following ultraviolet oxidation, in β-Bi_2SeO_5 film (top panel of Figure 1D), although the +3 oxidation state of Bi is retained, the binding energies of the Bi $4f_{7/2}$ and $4f_{5/2}$ peaks increased slightly to 158.84 eV and 164.12 eV, respectively, due to changes of the chemical environment. Meanwhile, the valence state of Se changed to +4 with the fitted signals of Se $3d_{5/2}$ and $3d_{3/2}$ shifting to 58.16 and 59.06 eV, respectively, which can be attributed to the formation of $[SeO_3]$ tetrahedra. In addition, the XRD and XPS results of a thicker (~13 nm) β-Bi_2SeO_5 film are shown in Figure S1, showing that Bi_2O_2Se was completely converted into β-Bi_2SeO_5.

In order to more intuitively observe the layer thickness after oxidation, we prepared ultrathin films with a thickness of 1-2 layers and measured the thickness of each single layer of β-Bi_2SeO_5 film using atomic force microscopy (AFM). As shown in Figure 2A, the color gradient from dark to light represents the $SrTiO_3$ substrate, the first-layer film, and the second-layer nucleus. We measured the height profile along the red line, which encompasses all three regions. The first and second layers of β-Bi_2SeO_5 exhibit an identical thickness of ~7.8 Å respectively, as shown in the line profile (Figure 2B), which corresponds to an interlayer distance of 7.8 Å in their crystal structure. A clearer comparison of the surface morphologies between β-Bi_2SeO_5 and the Bi_2O_2Se precursor prior to oxidation is presented in Figure S2. High-angle annular dark-

https://doi.org/10.1021/acs.nanolett.6c03261
Nano Lett. XXXX, XXX, XXX−XXX

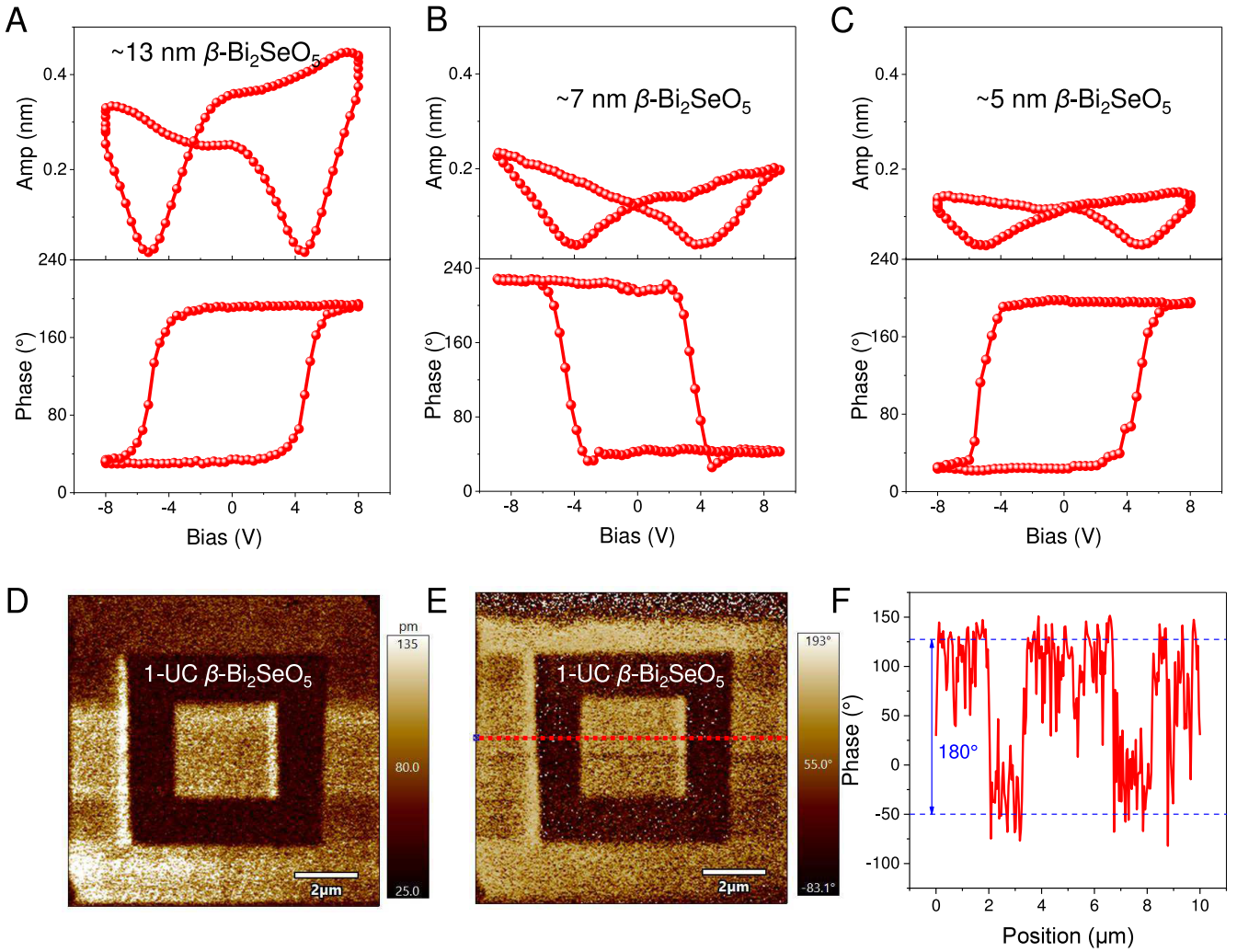

Figure 3. Characterization of out-of-plane ferroelectricity in multilayer β-Bi_2SeO_5 films. A) Off-field PFM phase (bottom) and amplitude (top) loops for β-Bi_2SeO_5 films with thickness of 13 nm, B) 7 nm and C) 5 nm, respectively. D) The PFM amplitude and E) phase images after opposite DC bias writing of "box-in-box" pattern of a 1-UC β-Bi_2SeO_5 film. F) The phase lag curve of the β-Bi_2SeO_5 at the red line position in (E).

field scanning transmission electron microscopy (HAADF-STEM) image reveals a well-defined crystal structure of the β-Bi_2SeO_5 film (Figure 2C). The layered β-Bi_2SeO_5 exhibits a stacking structure composed of alternating $[Bi_2O_2]^{2+}$ and $[SeO_3]^{2-}$ units, with out-of-plane and in-plane lattice constants of 7.8 Å and 3.9 Å, respectively (Figure 2D and 2E). These findings highlight the layered configuration and high crystalline quality of the β-Bi_2SeO_5 film, both of which are critical for investigating its FE properties.

To reveal the existence of room-temperature out-of-plane ferroelectricity in ultrathin β-Bi_2SeO_5 films, we used a dual AC resonance tracking piezoelectric force microscopy (PFM) measurement. The β-Bi_2SeO_5 was fabricated on a conductive Nb-doped $SrTiO_3$ (Nb-$SrTiO_3$) substrate and a tip/β-Bi_2SeO_5/Nb-$SrTiO_3$ structure was constructed for PFM measurements. We prepared a batch of β-Bi_2SeO_5 films with thickness of 13 nm, 7, 5, and 1.6 nm (1-UC), respectively. The thickness of thicker films was determined by X-ray reflectivity (XRR) fitting, whereas the thickness of the 1-UC film could not be reliably determined from this method. Additionally, because the 1-UC β-Bi_2SeO_5 structure is susceptible to degradation during STEM sample preparation, we utilized cross-sectional STEM characterization results of the monolayer Bi_2O_2Se prior to oxidation as supplementary evidence for determining the film thickness (Figure S4). The PFM results are depicted in Figure 3 and Figures S3 and S4. Off-field phase and amplitude loops were recorded for the 13 nm-thick film as illustrated in Figure 3A. A butterfly loop accompanied by 180° phase switching with a coercive voltage of approximately 4.3 V was observed, confirming out-of-plane ferroelectricity. For the 7 and 5 nm thick films, the coercive voltage remained nearly constant, whereas the amplitude decreased correspondingly with decreasing film thickness (Figure 3B and 3C). We then measured the writing and reading capabilities within a defined area in the 1-UC β-Bi_2SeO_5 film. When a DC voltage of ±8 V was applied to the 1-UC β-Bi_2SeO_5 thin film to write a "box-in-box" pattern, distinct light and dark regions were revealed by the PFM amplitude (Figure 3D) and phase (Figure 3E). And these areas exhibited a 180° phase difference (Figure 3F). The FE domains in 1-UC films are very stable, which we attribute to the absolutely flat surface of the ultrathin film. Furthermore, frequency-dependent PFM measurements were performed and showed good reproducibility (Figure S5), which can rule out electrostatic crosstalk and electrochemical effects during the PFM measurement.

https://doi.org/10.1021/acs.nanolett.6c03261
Nano Lett. XXXX, XXX, XXX−XXX

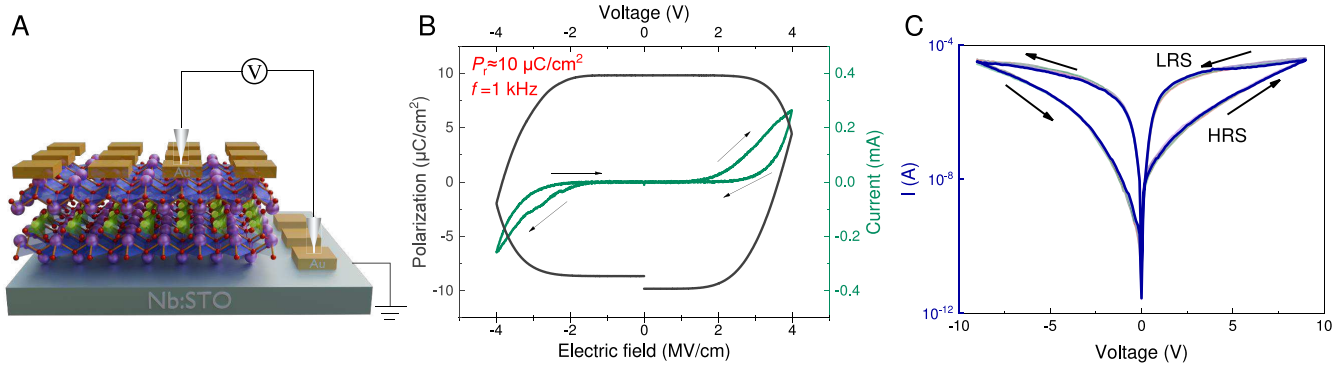

Figure 4. Macroscopic FE polarization and FE device characteristics of β-Bi_2SeO_5 films. A) Cross-sectional schematic of the β-Bi_2SeO_5 based ferroelectric measuring structure. B) The ferroelectric polarization−electric field hysteresis loop of the thin film, measured at an electric field frequency of 1 kHz. C) Sweep I−V curves (−9 V to +9 V) for the β-Bi_2SeO_5 based memristor.

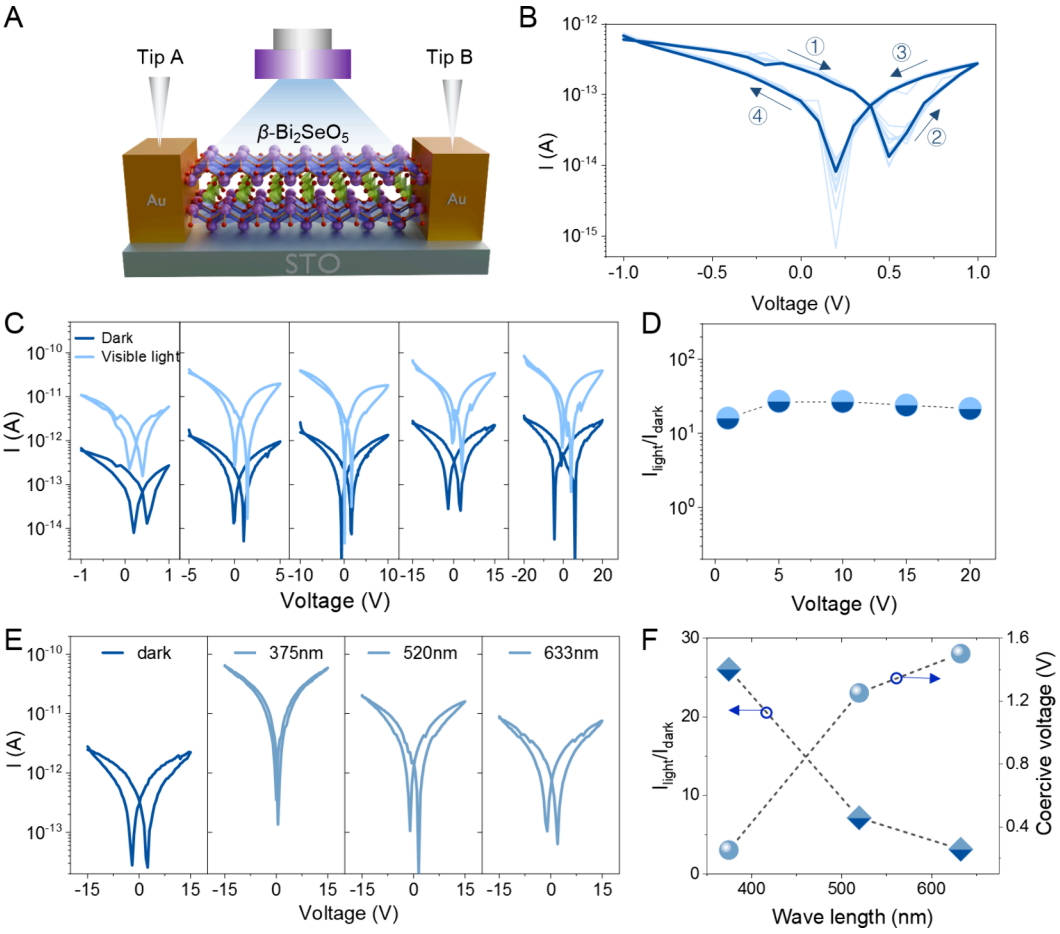

Figure 5. In-plane electrical and photoelectronic properties of β-Bi_2SeO_5 film. A) Schematic diagram of the in-plane electrical and optoelectronic device structure. B) In-plane I−V characteristic curve under a 1 V applied voltage. Measurements repeated ten times. C) Photocurrent versus dark current under visible light at 1, 5, 10, 15, and 20 V. D) Ratio of photocurrent to dark current under visible light. E) Photocurrent under laser irradiation at different wavelengths (375 nm, 520 nm, 633 nm), with dark current data provided for comparison. F) Ratio of photocurrent to dark current and V_C under laser irradiation at different wavelengths.

In addition to the microscopic ferroelectricity observed via PFM, the β-Bi_2SeO_5 thin films also demonstrate macroscopic ferroelectricity, as quantified using a FE analyzer. Figure 4A presents the test structure, where Au serves as the top electrode and Nb-doped $SrTiO_3$ as the bottom electrode. The optical image of the device is presented in Figure S6. Figure 4B shows the measured FE polarization-electric (P-E) hysteresis loop of a 10 nm thick β-Bi_2SeO_5 film, from which the key FE parameters were quantitatively extracted. Specifically, at an applied electric field of 4 V, the film exhibits a remnant polarization (P_r) of approximately 10 μC/cm^2. The film exhibits a relatively low leakage current density under the measured voltage, as illustrated in Figure S7, indicating that the observed polarization switching behavior is not dominated by leakage current contribution. The frequency-dependent P-E curves in the range of 100 Hz to 10 kHz are presented in

https://doi.org/10.1021/acs.nanolett.6c03261
Nano Lett. XXXX, XXX, XXX−XXX

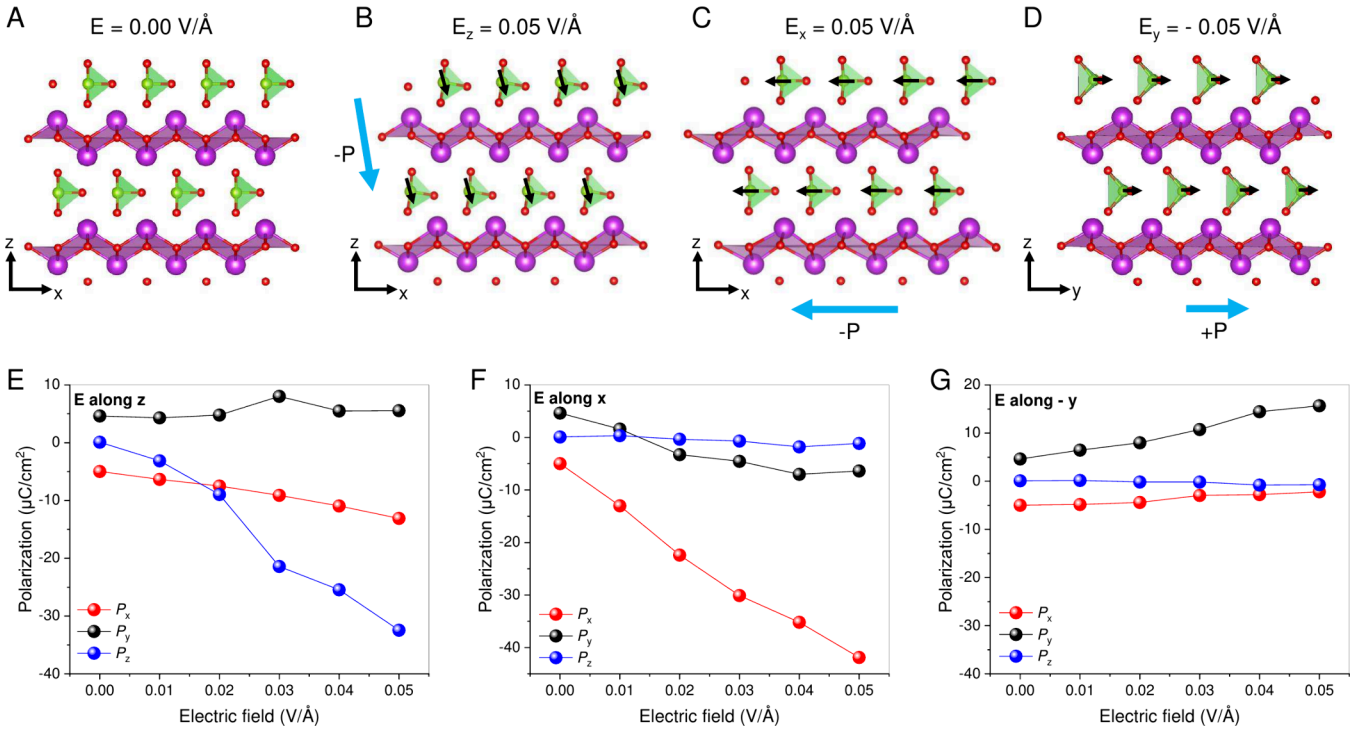

Figure 6. DFT simulations of the polar characteristics and underlying mechanism in β-Bi_2SeO_5 thin films. A) The original β-Bi_2SeO_5 crystal structure. B–D) β-Bi_2SeO_5 crystal structure with a 0.05 V/Å electric field applied along the z, x, and −y axes, respectively. E–G) The calculated polarization as a function of the electric field for the z, x, and −y directions, respectively.

Figure S8A. Figure S8B shows the full positive-up negative-down (PUND) switching current transients, wherein the peak of transient current response under triangular wave excitation exhibits a high intensity and narrow shape, further confirming the strong ferroelectricity of β-Bi_2SeO_5 thin film. The macroscopic FE hysteresis loop serves as direct evidence for the presence of out-of-plane polarization in the nanocomposite films, suggesting that these FE thin films hold significant potential for applications in electronic devices. We then further investigate the memristive effect induced by out-of-plane FE polarization. Figure 4C shows the current-voltage (I-V) characteristics under voltage sweeps ranging from -9 V to +9 V. The device switches from the initial high resistance state (HRS) to low resistance state (LRS) after a 0 to +9 V sweep, maintains LRS during the subsequent +9 V to −9 V scan, and returns to HRS from -9 to 0 V. These comprehensive analysis demonstrates the promising capabilities of the fabricated β-Bi_2SeO_5 films for advanced electronic applications.

In these layered β-Bi_2SeO_5 films, we also observed a pronounced in-plane ferroelectricity and photoelectric effect, along with a strong coupling between them. As shown in Figure S9, when a DC voltage of ±8 V was applied to write a zebra stripe pattern on the 7 nm β-Bi_2SeO_5 thin film, distinct bright and dark regions were revealed by the in-plane PFM amplitude and phase. The in-plane ferroelectricity has been further revealed by the in-plane transport measurements. As shown in Figure 5A, a two-terminal device was fabricated on β-Bi_2SeO_5 thin films grown on insulating $SrTiO_3$ substrates. As shown in Figure 5B, the I-V curve exhibits a well-defined butterfly shape, a characteristic signature predominantly attributable to the in-plane ferroelectricity of β-Bi_2SeO_5.[52] Notably, these I-V curves demonstrate excellent repeatability across multiple voltage sweep cycles, which serves as compelling experimental evidence for the robust intrinsic in-plane ferroelectricity within the β-Bi_2SeO_5 film. Furthermore, as shown by the dark blue curves in Figure 5C, the systematic measurements under different amplitudes of external electric field all exhibit a distinct butterfly-shaped profile, confirming that the FE response is stable and reproducible.

We subsequently investigated the photoelectric characteristics of the in-plane β-Bi_2SeO_5 device under illumination with visible light and monochromatic lasers of different wavelengths (375, 520, and 633 nm). As depicted in Figure 5C and 5D, the device exhibits pronounced photoelectric activity: under diverse in-plane voltage biases, the measured photocurrent is consistently one order of magnitude higher than the dark current, highlighting a strong light-matter interaction and efficient photo-induced charge carrier generation within the β-Bi_2SeO_5 film. Further wavelength-dependent photoelectric measurements, spanning from 375 to 633 nm, revealed that the device performance is highly sensitive to the excitation wavelength (Figure 5E). The time-dependent photocurrent curves are shown in Figure S10. Specifically, the β-Bi_2SeO_5 device achieves its peak photocurrent response at an excitation wavelength of 375 nm, where the photocurrent reaches 26 times higher than the dark current (Figure 5F). In contrast, the photocurrent response gradually diminishes as the excitation wavelength increases to 520 and 633 nm, which can be attributed to the reduced photon energy that fails to efficiently excite charge carriers across the bandgap. Concomitantly, a notable increase in the in-plane coercive voltage (V_C) was observed under identical applied voltage conditions as the laser wavelength increased (Figure 5F). The V_C value is defined as the difference between the two voltage values corresponding to $I_{off\ (min)}$ divided by 2. This phenomenon can be rationalized by the fact that short wavelength light irradiation provides additional photoexcitation energy to facilitate the switching of FE domains, thereby lowering the energy barrier for domain

https://doi.org/10.1021/acs.nanolett.6c03261
Nano Lett. XXXX, XXX, XXX−XXX

reversal and assisting the external electric field in driving the FE switching process, which consequently reduces the required V_C. Collectively, these results provide unambiguous experimental evidence for the concurrent existence of in-plane ferroelectricity and prominent photoelectronic properties in β-Bi_2SeO_5, as well as the strong coupling between these two functional attributes.

First-principles DFT simulations were implemented to explore the origin of ferroelectricity in β-Bi_2SeO_5 films. The pristine bulk β-Bi_2SeO_5 crystal exhibits an out-of-plane centrosymmetric structure with a zero net dipole moment and a non-centrosymmetric in-plane structure with an in-plane net dipole moment of ~5 $\mu C/cm^2$ (Figure 6A and 6E-F). Upon the application of vertical and in-plane electric fields, a pronounced directional displacement and distortion of the $[SeO_3]$ tetrahedra occur (Figure 6B-D). The pronounced polarization of β-Bi_2SeO_5 is attributed to the synergistic interaction between field-induced lattice deformation and local charge density redistribution. Calculation of the polarization along three axes revealed that P_x, P_y and P_z exhibit a monotonic positive dependence on the applied field strength, reaching values of −32.4 $\mu C/cm^2$ at 0.05 V/Å for P_z (Figure 6E), −41.8 $\mu C/cm^2$ at 0.05 V/Å for P_x (Figure 6F) and 15.6 $\mu C/cm^2$ at −0.05 V/Å for P_y (Figure 6G). The polarization opposite to the electric field direction is attributed to the negative charge of the $[SeO_3]$ tetrahedra. The calculated high polarization magnitude of β-Bi_2SeO_5 underscores the significant potential of its thin films for fabricating high-performance, low-power FE devices.

This work reports the controlled synthesis of single-crystalline β-Bi_2SeO_5 thin films via oxidation of high-quality, thickness-tunable Bi_2O_2Se precursors fabricated by MBE. The β-Bi_2SeO_5 films possess robust RT out-of-plane ferroelectricity, as verified by microscopic PFM and macroscopic FE analyzer, with an out-of-plane polarization of 10 $\mu C/cm^2$ for a 10 nm film. Besides out-of-plane ferroelectricity, the films also show in-plane ferroelectricity and remarkable optoelectronic responses, as well as strong coupling exists among these functional properties. First-principles DFT calculations indicate that the FE behavior of β-Bi_2SeO_5 stems from the displacement and distortion of $[SeO_3]$ tetrahedra under both out-of-plane and in-plane electric fields. These findings demonstrate that β-Bi_2SeO_5 is a promising candidate for multifunctional nanoelectronic and quantum devices, and lay a foundation for developing next-generation low-power, optically tunable ferroelectric devices.

■ ASSOCIATED CONTENT

Supporting Information

The Supporting Information is available free of charge at https://pubs.acs.org/doi/10.1021/acs.nanolett.6c03261.

Details of the experimental methods, XRD and XPS results for a 13 nm thick film, PFM results for a 7 nm thick film, characterization of a 1-UC film, frequency-dependent PFM results, an optical image of the FE devices, leakage current for a 10 nm thick film, frequency-dependent P-E curves and full PUND switching current transients for a 10 nm thick film, and in-plane PFM results for a 7 nm thick film (DOCX)

■ AUTHOR INFORMATION

Corresponding Authors

Jiandi Zhang − *Beijing National Laboratory for Condensed Matter Physics, Institute of Physics, Chinese Academy of Sciences, Beijing 100190, China; College of Physics, University of Chinese Academy of Sciences, Beijing 100190, China*; Email: jiandiz@iphy.ac.cn

Yan Liang − *Beijing National Laboratory for Condensed Matter Physics, Institute of Physics, Chinese Academy of Sciences, Beijing 100190, China*; orcid.org/0009-0003-8276-7845; Email: liangyan_sf6i@iphy.ac.cn

Pan Chen − *Beijing National Laboratory for Condensed Matter Physics, Institute of Physics, Chinese Academy of Sciences, Beijing 100190, China*; orcid.org/0009-0000-4997-0495; Email: panch@iphy.ac.cn

Runzhang Xu − *Department of Physics, The Hong Kong University of Science and Technology, Hong Kong 999077, China*; Email: xurz@ust.hk

Authors

Wei Li − *Beijing National Laboratory for Condensed Matter Physics, Institute of Physics, Chinese Academy of Sciences, Beijing 100190, China; Hebei Key Lab of Optic-electronic Information and Materials, College of Physics Science and Technology, Hebei University, Baoding 071002, China*

Lingyuan Kong − *Beijing National Laboratory for Condensed Matter Physics, Institute of Physics, Chinese Academy of Sciences, Beijing 100190, China; Hebei Key Lab of Optic-electronic Information and Materials, College of Physics Science and Technology, Hebei University, Baoding 071002, China*

Kai Hu − *Beijing National Laboratory for Condensed Matter Physics, Institute of Physics, Chinese Academy of Sciences, Beijing 100190, China*

Long Chen − *Beijing National Laboratory for Condensed Matter Physics, Institute of Physics, Chinese Academy of Sciences, Beijing 100190, China*

Tianci Hu − *Beijing National Laboratory for Condensed Matter Physics, Institute of Physics, Chinese Academy of Sciences, Beijing 100190, China*

Zeguo Lin − *Beijing National Laboratory for Condensed Matter Physics, Institute of Physics, Chinese Academy of Sciences, Beijing 100190, China*; orcid.org/0009-0001-2678-8735

Yi Jiang − *Beijing National Laboratory for Condensed Matter Physics, Institute of Physics, Chinese Academy of Sciences, Beijing 100190, China*

Fang Yang − *Beijing National Laboratory for Condensed Matter Physics, Institute of Physics, Chinese Academy of Sciences, Beijing 100190, China*; orcid.org/0000-0003-4855-585X

Jiandong Guo − *Beijing National Laboratory for Condensed Matter Physics, Institute of Physics, Chinese Academy of Sciences, Beijing 100190, China; College of Physics, University of Chinese Academy of Sciences, Beijing 100190, China*; orcid.org/0000-0002-7893-022X

Yang Guo − *Beijing National Laboratory for Condensed Matter Physics, Institute of Physics, Chinese Academy of Sciences, Beijing 100190, China*; orcid.org/0000-0001-8975-9387

Wei Zhang − *Hebei Key Lab of Optic-electronic Information and Materials, College of Physics Science and Technology,*

Hebei University, Baoding 071002, China; orcid.org/0000-0002-4786-7045

Complete contact information is available at: https://pubs.acs.org/10.1021/acs.nanolett.6c03261

Notes

The authors declare no competing financial interest.

■ ACKNOWLEDGMENTS

This work was supported by the National Key Research and Development Program of China (Grant No. 2024YFF0508500, 2022YFA1403000), the National Natural Science Foundation of China (Grant No. 12434007 and U23A20366) and the CAS Project for Young Scientists in Basic Research (YSBR-143).

■ REFERENCES

(1) Valasek, J. Piezo-Electric and Allied Phenomena in Rochelle Salt. *Phys. Rev.* **1921**, *17* (4), 475−481.
(2) Wu, M. 100 Years of Ferroelectricity. *Nat. Rev. Phys.* **2021**, *3* (11), 726−726.
(3) Wang, C.; You, L.; Cobden, D.; Wang, J. Towards Two-Dimensional van Der Waals Ferroelectrics. *Nat. Mater.* **2023**, *22* (5), 542−552.
(4) Feng, G.; Zhu, Q.; Liu, X.; Chen, L.; Zhao, X.; Liu, J.; Xiong, S.; Shan, K.; Yang, Z.; Bao, Q.; Yue, F.; Peng, H.; Huang, R.; Tang, X.; Jiang, J.; Tang, W.; Guo, X.; Wang, J.; Jiang, A.; Dkhil, B.; Tian, B.; Chu, J.; Duan, C. A Ferroelectric Fin Diode for Robust Non-Volatile Memory. *Nat. Commun.* **2024**, *15* (1), 513.
(5) Peng, Y.; Liu, X.; Luo, G.; Zhang, F.; Sun, T.; Li, H.; Cheng, Y.; Peng, Y. Flexible $BaTiO_3$ Ferroelectric Nonvolatile Memory for Neuromorphic Computation. *ACS Appl. Mater. Interfaces* **2025**, *17* (12), 18571−18581.
(6) Liu, Y.; Tang, W.; Zeng, J.; Bai, C.; Zhou, K.; Zhang, X.; Liu, Q.; Huang, Z.; Wu, G.; Wang, J. Ferroelectric-Based Neuromorphic Memory Devices for Bio-Inspired Computing. *Nat. Rev. Electr. Eng.* **2025**, *2* (11), 773−787.
(7) Wu, Q.; Li, Z.; Han, B.; Sun, W.; Liu, Q.; Xue, C.; Bae, H.; Wang, M.; Fu, B.; Qian, J.; Zhu, Y.; Sun, Y.; Feng, T.; Gao, X.; Cong, X.; Liu, W.; Gao, Y.; Yan, B.; Tan, C.; Liu, H.; Peng, H. Wafer-Scale Ultrathin and Uniform van Der Waals Ferroelectric Oxide. *Science* **2026**, *391* (6784), No. eadz1655.
(8) Yoo, S.; Kim, T. J.; Nam, S.-G.; Kim, D.; Kim, K.; Lee, Y.; Jung, M.; Lee, K.-H.; Choi, S.; Hyun, S. D.; Lee, M.-H.; Hong, S.; Kim, H.; Bae, K. D.; Lee, H.; Won, J. Y.; Yun, D.-J.; Chae, B. G.; Hahn, W. G.; Joo, C. H.; Jo, S.; Park, Y.; Song, K. M.; Jung, K.; Lim, S.; Seo, K.; Kim, K.; Kim, W.; Ha, D.; Yang, J.-E.; Yang, S.-Y.; Kim, S.; Heo, J.; Choe, D.-H. Ferroelectric Transistors for Low-Power NAND Flash Memory. *Nature* **2025**, *648* (8093), 320−326.
(9) Si, M.; Saha, A. K.; Gao, S.; Qiu, G.; Qin, J.; Duan, Y.; Jian, J.; Niu, C.; Wang, H.; Wu, W.; Gupta, S. K.; Ye, P. D. A Ferroelectric Semiconductor Field-Effect Transistor. *Nat. Electron.* **2019**, *2* (12), 580−586.
(10) Tan, C.; Tang, J.; Gao, X.; Xue, C.; Peng, H. 2D Bismuth Oxyselenide Semiconductor for Future Electronics. *Nat. Rev. Electr. Eng.* **2025**, *2* (7), 494−513.
(11) Qiu, C.; Zhang, Z.; Xu, Z.; Qiao, L.; Ning, L.; Zhang, S.; Su, M.; Wu, W.; Song, K.; Xu, Z.; Chen, L.-Q.; Zheng, H.; Liu, C.; Qiu, W.; Li, F. Transparent Ultrasonic Transducers Based on Relaxor Ferroelectric Crystals for Advanced Photoacoustic Imaging. *Nat. Commun.* **2024**, *15* (1), 10580.
(12) Petritz, A.; Karner-Petritz, E.; Uemura, T.; Schäffner, P.; Araki, T.; Stadlober, B.; Sekitani, T. Imperceptible Energy Harvesting Device and Biomedical Sensor Based on Ultraflexible Ferroelectric Transducers and Organic Diodes. *Nat. Commun.* **2021**, *12* (1), 2399.
(13) Zhou, X.; Zhang, J.; Luo, H.; Zhang, Y.; Tang, S.; Huang, H.; Yuan, X.; Song, M.; Qi, H.; Zhang, D. Lead-Free Ferroelectrics with Giant Unipolar Strain for High-Precision Actuators. *Nat. Commun.* **2024**, *15* (1), 6625.
(14) Liu, Y.; Zhou, Y.; Qin, H.; Yang, T.; Chen, X.; Li, L.; Han, Z.; Wang, K.; Zhang, B.; Lu, W.; Chen, L.-Q.; Bernholc, J.; Wang, Q. Electro-Thermal Actuation in Percolative Ferroelectric Polymer Nanocomposites. *Nat. Mater.* **2023**, *22* (7), 873−879.
(15) Sawyer, C. B. The Use of Rochelle Salt Crystals for Electrical Reproducers and Microphones. *Proc. IRE* **1931**, *19* (11), 2020−2029.
(16) Cochran, W. Crystal Stability and the Theory of Ferroelectricity. *Adv. Phys.* **1960**, *9* (36), 387−423.
(17) Sun, H.; Chen, P.; Mao, W.; Guo, C.; Li, Y.; Wang, J.; Sun, W.; Xu, D.; Hao, B.; Zhang, T.; Ma, J.; Yang, J.; Cao, Z.; Yan, S.; Guan, Y.; Wen, Z.; Mao, Z.; Zheng, N.; Gu, Z.; Huang, H.; Wang, P.; Zhang, Y.; Wu, D.; Nie, Y. Ferroelectric Topologies in $BaTiO_3$ Nanomembranes for Light Field Manipulation. *Nat. Nanotechnol.* **2025**, *20* (7), 881−888.
(18) Yang, X.; Han, L.; Ning, H.; Xu, S.; Hao, B.; Li, Y.-C.; Li, T.; Gao, Y.; Yan, S.; Li, Y.; Gu, C.; Li, W.; Gu, Z.; Lun, Y.; Shi, Y.; Zhou, J.; Hong, J.; Wang, X.; Wu, D.; Nie, Y. Ultralow-Pressure-Driven Polarization Switching in Ferroelectric Membranes. *Nat. Commun.* **2024**, *15* (1), 9281.
(19) Nelson, C. T.; Gao, P.; Jokisaari, J. R.; Heikes, C.; Adamo, C.; Melville, A.; Baek, S.-H.; Folkman, C. M.; Winchester, B.; Gu, Y.; Liu, Y.; Zhang, K.; Wang, E.; Li, J.; Chen, L.-Q.; Eom, C.-B.; Schlom, D. G.; Pan, X. Domain Dynamics During Ferroelectric Switching. *Science* **2011**, *334* (6058), 968−971.
(20) Xu, X.; Wang, T.; Chen, P.; Zhou, C.; Ma, J.; Wei, D.; Wang, H.; Niu, B.; Fang, X.; Wu, D.; Zhu, S.; Gu, M.; Xiao, M.; Zhang, Y. Femtosecond Laser Writing of Lithium Niobate Ferroelectric Nanodomains. *Nature* **2022**, *609* (7927), 496−501.
(21) Martin, L. W.; Rappe, A. M. Thin-Film Ferroelectric Materials and Their Applications. *Nat. Rev. Mater.* **2017**, *2* (2), 16087.
(22) Sun, H.; Gu, J.; Li, Y.; Paudel, T. R.; Liu, D.; Wang, J.; Zang, Y.; Gu, C.; Yang, J.; Sun, W.; Gu, Z.; Tsymbal, E. Y.; Liu, J.; Huang, H.; Wu, D.; Nie, Y. Prominent Size Effects without a Depolarization Field Observed in Ultrathin Ferroelectric Oxide Membranes. *Phys. Rev. Lett.* **2023**, *130*, 126801.
(23) Fong, D. D.; Stephenson, G. B.; Streiffer, S. K.; Eastman, J. A.; Auciello, O.; Fuoss, P. H.; Thompson, C. Ferroelectricity in Ultrathin Perovskite Films. *Science* **2004**, *304* (5677), 1650−1653.
(24) Guan, Z.; Hu, H.; Shen, X.; Xiang, P.; Zhong, N.; Chu, J.; Duan, C. Recent Progress in Two-Dimensional Ferroelectric Materials. *Adv. Electron. Mater.* **2020**, *6* (1), 1900818.
(25) Chi, M.; Zhang, X.; Liu, J.; Wang, Y.; Yu, A.; Guo, D.; Zhai, J. Emerging 2D Ferroelectric Semiconductors: From Fundamentals to Advanced Device Applications. *Adv. Sci.* **2025**, *12* (47), No. e14185.
(26) Chen, J.; Liu, Z.; Dong, X.; Gao, Z.; Lin, Y.; He, Y.; Duan, Y.; Cheng, T.; Zhou, Z.; Fu, H.; Luo, F.; Wu, J. Vertically Grown Ultrathin Bi_2SiO_5 as High-κ Single-Crystalline Gate Dielectric. *Nat. Commun.* **2023**, *14* (1), 4406.
(27) Kong, L.; Li, W.; Wang, Z.; Fan, Z.; Yin, Z.; Ling, H.; Hu, K.; Tai, S.; Li, D.; Li, C.; Guo, Y.; Yang, F.; Zhang, W.; Guo, J.; Xu, R.; Chen, P.; Liang, Y.; Zhang, J. Room-Temperature Ferroelectricity in Ultra-Thin p-Type BiCuSeO Films. *Adv. Mater.* **2025**, *37* (45), No. e10566.
(28) Shang, Z.; Liu, L.; Wang, G.; Xu, H.; Cui, Y.; Deng, J.; Lou, Z.; Yan, Y.; Deng, J.; Han, S.-T.; Zhai, T.; Wang, X.; Wang, L.; Wang, X. Ferroelectric Polarization Enhanced Optoelectronic Synaptic Response of a $CuInP_2S_6$ Transistor Structure. *ACS Nano* **2024**, *18* (44), 30530−30539.
(29) Liu, K.; Zhang, T.; Dang, B.; Bao, L.; Xu, L.; Cheng, C.; Yang, Z.; Huang, R.; Yang, Y. An Optoelectronic Synapse Based on α-In_2Se_3 with Controllable Temporal Dynamics for Multimode and Multiscale Reservoir Computing. *Nat. Electron.* **2022**, *5* (11), 761−773.
(30) Pei, Y.; Shang, Y.; Liu, G.; Ma, S.; Guo, M.; Liu, C.; Hou, Y.; Wang, F.; Wang, J.; Liu, D.; Zhao, J.; Guo, J.; Yan, X. Zn^{2+} Engineered Low-Barrier $LiNbO_3$ Enables Visible-Light Programmable Ferro-

electric Memristors for Noise-Immune Neuromorphic Vision. *Adv. Mater.* **2026**, *38*, No. e11352.
(31) Liu, F.; You, L.; Seyler, K. L.; Li, X.; Yu, P.; Lin, J.; Wang, X.; Zhou, J.; Wang, H.; He, H.; Pantelides, S. T.; Zhou, W.; Sharma, P.; Xu, X.; Ajayan, P. M.; Wang, J.; Liu, Z. Room-Temperature Ferroelectricity in $CuInP_2S_6$ Ultrathin Flakes. *Nat. Commun.* **2016**, *7* (1), 12357.
(32) Park, C. B.; Shahee, A.; Kim, K.; Patil, D. R.; Guda, S. A.; Ter-Oganessian, N.; Kim, K. H. Observation of Spin-Induced Ferroelectricity in a Layered van Der Waals Antiferromagnet $CuCrP_2S_6$. *Adv. Electron. Mater.* **2022**, *8* (6), 2101072.
(33) Han, W.; Zheng, X.; Yang, K.; Tsang, C. S.; Zheng, F.; Wong, L. W.; Lai, K. H.; Yang, T.; Wei, Q.; Li, M.; Io, W. F.; Guo, F.; Cai, Y.; Wang, N.; Hao, J.; Lau, S. P.; Lee, C.-S.; Ly, T. H.; Yang, M.; Zhao, J. Phase-Controllable Large-Area Two-Dimensional In_2Se_3 and Ferroelectric Heterophase Junction. *Nat. Nanotechnol.* **2023**, *18* (1), 55−63.
(34) Song, Q.; Occhialini, C. A.; Ergeçen, E.; Ilyas, B.; Amoroso, D.; Barone, P.; Kapeghian, J.; Watanabe, K.; Taniguchi, T.; Botana, A. S.; Picozzi, S.; Gedik, N.; Comin, R. Evidence for a Single-Layer van Der Waals Multiferroic. *Nature* **2022**, *602* (7898), 601−605.
(35) Chang, K.; Liu, J.; Lin, H.; Wang, N.; Zhao, K.; Zhang, A.; Jin, F.; Zhong, Y.; Hu, X.; Duan, W.; Zhang, Q.; Fu, L.; Xue, Q.-K.; Chen, X.; Ji, S.-H. Discovery of Robust In-Plane Ferroelectricity in Atomic-Thick SnTe. *Science* **2016**, *353* (6296), 274−278.
(36) Varotto, S.; Nessi, L.; Cecchi, S.; Sławińska, J.; Noël, P.; Petrò, S.; Fagiani, F.; Novati, A.; Cantoni, M.; Petti, D.; Albisetti, E.; Costa, M.; Calarco, R.; Buongiorno Nardelli, M.; Bibes, M.; Picozzi, S.; Attané, J.-P.; Vila, L.; Bertacco, R.; Rinaldi, C. Room-Temperature Ferroelectric Switching of Spin-to-Charge Conversion in Germanium Telluride. *Nat. Electron.* **2021**, *4* (10), 740−747.
(37) Wang, X.; Yasuda, K.; Zhang, Y.; Liu, S.; Watanabe, K.; Taniguchi, T.; Hone, J.; Fu, L.; Jarillo-Herrero, P. Interfacial Ferroelectricity in Rhombohedral-Stacked Bilayer Transition Metal Dichalcogenides. *Nat. Nanotechnol.* **2022**, *17* (4), 367−371.
(38) Yuan, S.; Luo, X.; Chan, H. L.; Xiao, C.; Dai, Y.; Xie, M.; Hao, J. Room-Temperature Ferroelectricity in $MoTe_2$ down to the Atomic Monolayer Limit. *Nat. Commun.* **2019**, *10* (1), 1775.
(39) Kong, L.; Li, W.; Hu, K.; Fan, Z.; Yin, Z.; Ling, H.; Wang, Z.; Li, D.; Tai, S.; Li, C.; Jabeen, F.; Guo, Y.; Xu, R.; Yang, F.; Guo, J.; Zhang, W.; Chen, P.; Liang, Y.; Zhang, J. Room-Temperature Ferroelectricity of Bi_2O_2Se in the Two-Dimensional Limit. *Nano Lett.* **2025**, *25* (51), 17636−17643.
(40) Wu, J.; Yuan, H.; Meng, M.; Chen, C.; Sun, Y.; Chen, Z.; Dang, W.; Tan, C.; Liu, Y.; Yin, J.; Zhou, Y.; Huang, S.; Xu, H. Q.; Cui, Y.; Hwang, H. Y.; Liu, Z.; Chen, Y.; Yan, B.; Peng, H. High Electron Mobility and Quantum Oscillations in Non-Encapsulated Ultrathin Semiconducting Bi_2O_2Se. *Nat. Nanotechnol.* **2017**, *12* (6), 530−534.
(41) Liang, Y.; Chen, Y.; Sun, Y.; Xu, S.; Wu, J.; Tan, C.; Xu, X.; Yuan, H.; Yang, L.; Chen, Y.; Gao, P.; Guo, J.; Peng, H. Molecular Beam Epitaxy and Electronic Structure of Atomically Thin Oxyselenide Films. *Adv. Mater.* **2019**, *31* (39), 1901964.
(42) Zhang, C.; Tu, T.; Wang, J.; Zhu, Y.; Tan, C.; Chen, L.; Wu, M.; Zhu, R.; Liu, Y.; Fu, H.; Yu, J.; Zhang, Y.; Cong, X.; Zhou, X.; Zhao, J.; Li, T.; Liao, Z.; Wu, X.; Lai, K.; Yan, B.; Gao, P.; Huang, Q.; Xu, H.; Hu, H.; Liu, H.; Yin, J.; Peng, H. Single-Crystalline van Der Waals Layered Dielectric with High Dielectric Constant. *Nat. Mater.* **2023**, *22* (7), 832−837.
(43) Tan, C.; Yu, M.; Tang, J.; Gao, X.; Yin, Y.; Zhang, Y.; Wang, J.; Gao, X.; Zhang, C.; Zhou, X.; Zheng, L.; Liu, H.; Jiang, K.; Ding, F.; Peng, H. 2D Fin Field-Effect Transistors Integrated with Epitaxial High-k Gate Oxide. *Nature* **2023**, *616* (7955), 66−72.
(44) Xue, C.; Tan, C.; Gao, X.; Tang, J.; Sun, W.; Yin, Y.; Wang, M.; Gao, X.; An, H.; Fu, B.; Liu, W.; Wang, Y.; Li, Y.; Ding, F.; Peng, H. Wafer-Scale Uniform Epitaxy of Transferable 2D Single Crystals for Gate-All-around Nanosheet Field Effect Transistors. *Nat. Commun.* **2025**, *16* (1), 10587.
(45) Zhao, Y.; Lou, Z.; Hu, J.; Li, Z.; Xu, L.; Chen, Z.; Xu, Z.; Wang, T.; Wu, M.; Ying, H.; An, M.; Li, W.; Lin, X.; Zheng, X. Scalable Layer-Controlled Oxidation of Bi_2O_2Se for Self-Rectifying Memristor Arrays With sub-pA Sneak Currents. *Adv. Mater.* **2024**, *36* (44), 2406608.
(46) Zhang, Y.; Yu, J.; Zhu, R.; Wang, M.; Tan, C.; Tu, T.; Zhou, X.; Zhang, C.; Yu, M.; Gao, X.; Wang, Y.; Liu, H.; Gao, P.; Lai, K.; Peng, H. A Single-Crystalline Native Dielectric for Two-Dimensional Semiconductors with an Equivalent Oxide Thickness below 0.5 nm. *Nat. Electron.* **2022**, *5* (10), 643−649.
(47) Tang, J.; Jiang, J.; Gao, X.; Gao, X.; Zhang, C.; Wang, M.; Xue, C.; Li, Z.; Yin, Y.; Tan, C.; Ding, F.; Qiu, C.; Peng, L.-M.; Peng, H. Low-Power 2D Gate-All-around Logics via Epitaxial Monolithic 3D Integration. *Nat. Mater.* **2025**, *24* (4), 519−526.
(48) Zhao, Y.; Hu, J.; Lou, Z.; Xu, L.; Li, W.; Lin, X.; Zheng, X. Defect Engineering in β-Bi_2SeO_5/Bi_2O_2Se Heterostructures for High-Resolution Phototransistor Arrays. *Adv. Mater.* **2026**, *38*, No. e17425.
(49) Zhou, X.; Liang, Y.; Fu, H.; Zhu, R.; Wang, J.; Cong, X.; Tan, C.; Zhang, C.; Zhang, Y.; Wang, Y.; Xu, Q.; Gao, P.; Peng, H. Step-Climbing Epitaxy of Layered Materials with Giant Out-of-Plane Lattice Mismatch. *Adv. Mater.* **2022**, *34* (42), 2202754.
(50) Song, Y.; Li, Z.; Li, H.; Tang, S.; Mu, G.; Xu, L.; Peng, W.; Shen, D.; Chen, Y.; Xie, X.; Jiang, M. Epitaxial Growth and Characterization of High Quality Bi_2O_2Se Thin Films on $SrTiO_3$ Substrates by Pulsed Laser Deposition. *Nanotechnology* **2020**, *31* (16), 165704.
(51) Kang, M.; Chai, H.-J.; Jeong, H. B.; Park, C.; Jung, I.; Park, E.; Çiçek, M. M.; Lee, I.; Bae, B.-S.; Durgun, E.; Kwak, J. Y.; Song, S.; Choi, S.-Y.; Jeong, H. Y.; Kang, K. Low-Temperature and High-Quality Growth of Bi_2O_2Se Layered Semiconductors via Cracking Metal−Organic Chemical Vapor Deposition. *ACS Nano* **2021**, *15* (5), 8715−8723.
(52) Hao, Z.; Zhao, G.; Liu, J.; Tong, Y.; Li, H.; Zhang, J.; Liu, J.; Kong, F.; Kozadaev, K. V.; Li, Y.; Han, X.; Li, H.; Huang, H.; Sun, C.; Tolstik, A.; Novitsky, A.; Pan, L.; Li, D. Observation of Intrinsic and LED Light-Enhanced Memristor Performance in In-Plane Ferroelectric $NbOI_2$. *ACS Nano* **2025**, *19* (30), 27654−27664.

https://doi.org/10.1021/acs.nanolett.6c03261
Nano Lett. XXXX, XXX, XXX−XXX